Chinese Chemical Letters 35 (2024) 109029

Contents lists available at ScienceDirect

Chinese Chemical Letters

journal homepage: www.elsevier.com/locate/cclet

Microenvironment responsive pod-structured astaxanthin nanocarrier for ameliorating inflammatory bowel disease

Jingting Wang[a,1], Yuanyuan Chen[b,1], Linlin Han[a], Shasha Xia[b], Xingyao Zhang[a], Peng Xue[a], Yuejun Kang[a], Jian Ming[b,*], Zhigang Xu[a,c,*]

[a] Key Laboratory of Luminescence Analysis and Molecular Sensing, Ministry of Education, School of Materials and Energy & Chongqing Engineering Research Center for Micro-Nano Biomedical Materials and Devices, Southwest University, Chongqing 400715, China
[b] College of Food Science, Southwest University, Chongqing 400715, China
[c] State Key Laboratory of Chemo/Biosensing and Chemometrics, Hunan University, Changsha 410082, China

ARTICLE INFO

Article history:
Received 19 July 2023
Revised 25 August 2023
Accepted 31 August 2023
Available online 3 September 2023

Keywords:
Oral administration
Astaxanthin
Nanocarrier
Anti-oxidant activity
Colon targeting

ABSTRACT

Anti-inflammatory drugs targeting inflammatory bowel disease (IBD) have attracted considerable attention but still face low therapeutic outcomes and frequent side effects. Astaxanthin (ATX), a natural ketone, possesses potent antioxidant and anti-inflammatory properties. However, it faces problems such as poor water solubility, photothermal instability, and low bioavailability. Here, we employed a supramolecular encapsulation strategy to create a nanoscale oral delivery system for ATX (referred to as FC-ATX NPs) by coupling fucoidan (FUC) with chitosan oligosaccharides (COS). The obtained FC-ATX NPs exhibited a particular "bean pod" structure with uniform size, good encapsulation efficiency, excellent physical and chemical stability, pH-triggered intestinal targeted slow-release properties, and potent antioxidant capacity. *In vitro* cell culture experiments showed that FC-ATX NPs promoted cellular uptake and scavenged excessive intracellular reactive oxygen species (ROS). In mouse models of colitis, FC-ATX NPs enhanced the drug absorption of intestinal epithelial cells and effectively accumulated at the site of inflammation. This work provides an efficient approach to enhance the bioavailability of ATX and has excellent application potential as an oral targeted delivery system for colitis therapy.

Inflammatory bowel disease (IBD) represents a chronic gastrointestinal inflammation comprising ulcerative colitis and Crohn's disease [1]. IBD can induce intestinal microbial dysbiosis, intestinal mucosal barrier dysfunction, pathological cytokine production, and immune function decline [2]. Long-term diarrhea in patients can result in weight loss and malnutrition. Furthermore, patients predisposed to IBD have a higher probability of developing colitis-associated cancers [3]. Excessive production of reactive oxygen species (ROS), such as superoxide anions (O^{2-}), singlet oxygen ($O_2{}^1$), hydrogen peroxide (H_2O_2), and hydroxyl radicals ($^{\bullet}OH$), is one of the main contributing factors to IBD [4,5]. Therefore, therapy based on antioxidants capable of regulating the balance between oxidation and antioxidants can be one of the effective strategies for colitis therapy.

Currently, the therapy of IBD mainly relies on antibiotics, aminosalicylates, and corticosteroids [6]. However, these drugs lack specificity in targeted therapy, leading to reduced efficacy of the drugs and potential adverse reactions in other organs [7]. It is valuable to create intelligent drug-delivery systems that specifically target the intestine [8,9]. Innovative carriers based on pH and redox stimuli have been gradually designed and applied in constructing colon-specific delivery systems [10–13]. Compared to intravenous injection and subcutaneous administration, oral nano-delivery therapy for IBD reduces high medical costs and achieves rapid and precise drug targeting, thereby improving therapy efficiency [7,14].

Astaxanthin (ATX) belongs to the xanthophyll family of carotenoids [15,16] and is a ketone compound with a chemical structure encompassing numerous unsaturated carbon chains, ketone groups, and hydroxyl groups [17–19]. These unsaturated structures can quench singlet oxygen and scavenge free radicals, giving ATX high antioxidant and anti-inflammatory bioactivity [20,21]. However, exposure to adverse conditions, such as high temperature, oxygen, light, and extreme pH, can induce the chemical oxidation of ATX, resulting in degradation and loss of its biological activity [21,22]. Extensive research has been conducted on delivery systems for ATX to enhance its hydrophilicity, stability, and

* Corresponding authors.
E-mail addresses: food_mj@swu.edu.cn (J. Ming), zgxu@swu.edu.cn (Z. Xu).
[1] These authors contributed equally to this work.

https://doi.org/10.1016/j.cclet.2023.109029
1001-8417/

bioavailability due to its low solubility in water [23]. However, ATX is prone to decomposition in the stomach's highly acidic environment [24], leading to poor intestinal absorption, so there are still some limitations in the oral drug delivery system of ATX [25–27]. Therefore, constructing intelligent stimuli-responsive nano-delivery systems capable of withstanding acid decomposition is an effective strategy to improve the efficacy of ATX in colitis therapy.

Moreover, the delivery system's surface charge can influence nanoparticle entry into the intestinal mucosa [1,28]. Due to the high content of cationic proteins on the surface of inflammatory intestinal epithelial cells and in the microenvironment, negatively charged delivery systems tend to accumulate at inflammatory sites [29]. Fucoidan (FUC), a sulfated amphiphilic marine polysaccharide with a negative charge [30], has been widely employed in constructing intelligent, responsive delivery systems due to its ionizable sulfonic acid groups [31]. Compared to other sulfated polysaccharides, FUC is widely available, cost-effective, and exhibits higher antioxidant and free radical scavenging activities [32,33]. Chitosan oligosaccharide (COS), derived from the hydrolysis of chitosan (CS) [34], is a low molecular weight polymer resulting from partial deacetylation of chitin [35]. Unlike CS, which relies on acid solutions or structural alterations to enhance solubility, COS possesses the advantages of low viscosity and high-water solubility [36,37]. Additionally, COS contains abundant amino groups, conferring a positive charge on COS under a weakly acidic environment [38,39]. This positive charge enables COS to interact with many negatively charged polyelectrolytes, forming complexes or conjugates [40,41]. Moreover, the amino groups of COS display obvious protonation and deprotonation effects in acid-base environments, facilitating the construction of carriers with pH-responsive properties [42,43]. Therefore, the self-assembly of FUC and COS offers a promising way to prepare green, safe, simple and effective nanocarriers.

In this study, we designed and prepared pH-responsive release nanoparticles (Fig. 1A). Fucoidan and chitosan oligosaccharide self-assembled through ultrasound to form the ATX-loaded nanoscale delivery system (FC-ATX NPs). The resulting FC-ATX NPs, which exhibit high stability under acidic conditions while degrading under neutral and alkaline conditions, avoid significant release of ATX in the stomach during oral therapy and enable targeted drug delivery to the colon (Figs. 1B and C). Moreover, the antioxidant and anti-inflammatory properties of FC-ATX NPs can effectively treat dextran sodium sulfate (DSS)-induced colitis, thus realizing the efficient absorption and utilization of ATX in the intestines.

We adjusted the composition ratio during preparation to obtain nanoparticles (NPs) with small particle sizes and relatively high drug loading. When the molar ratio of FUC:COS was 1:1, FC NPs exhibited the optimal particle size and dispersity (Table S1 in Supporting information). Therefore, we selected a carrier ratio of

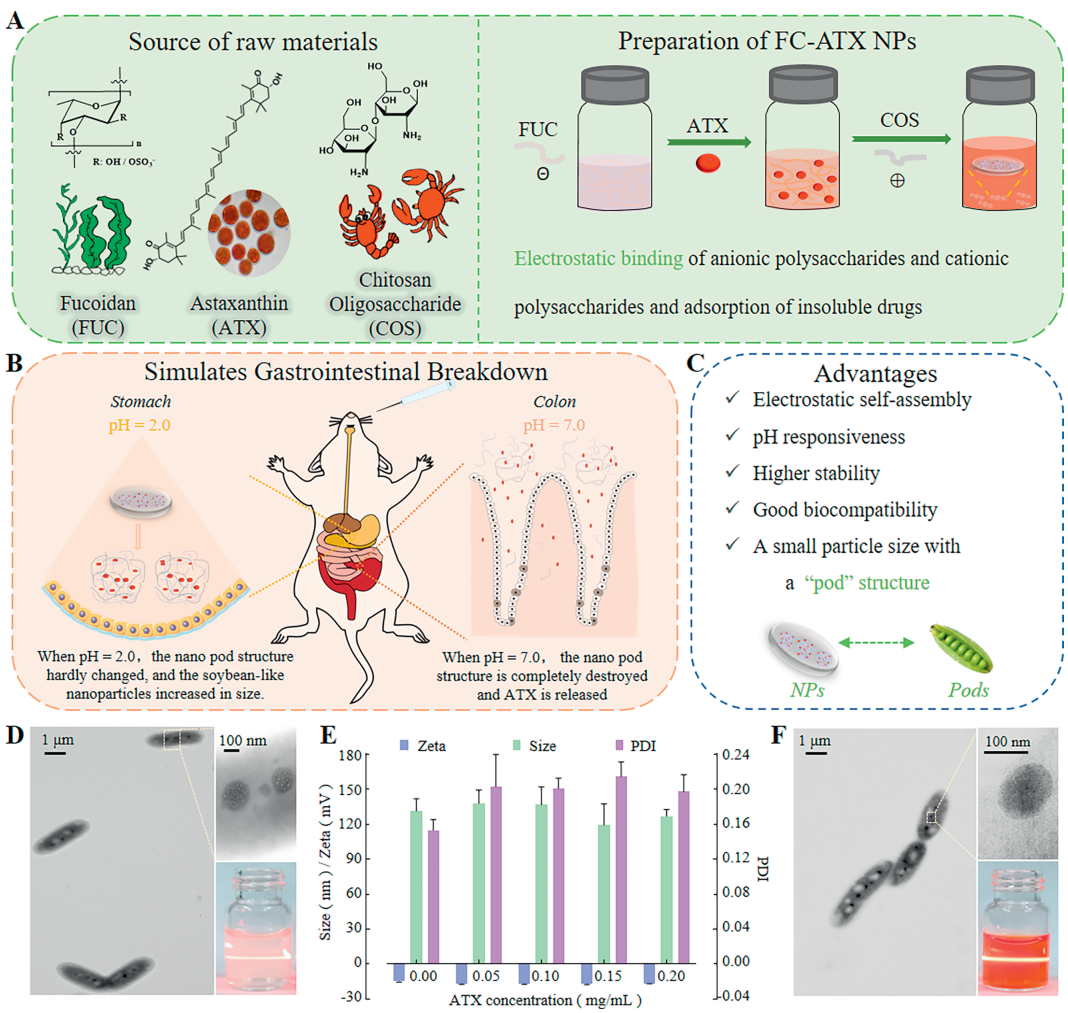

Fig. 1. Proportional exploration and characterization of FC-ATX NPs. (A) Material source and synthesis of FC-ATX NPs. (B) Schematic diagram of gastrointestinal release in a mouse model. (C) Advantages of FC-ATX NPs. (D) TEM and material images of FC NPs, with a scale of 1 μm and an illustration scale of 100 nm. (E) DLS data of different proportions of FC-ATX NPs. (F) TEM and material images of FC-ATX NPs, with a scale of 1 μm and an illustration scale of 100 nm. Data are presented as mean ± standard deviation (SD) ($n = 3$).

1:1 for FUC to COS. The transmission electron microscope (TEM) images of FC NPs unveiled a distinctive pod-shaped structure, with the nanoparticles exhibiting the Tyndall effect upon laser illumination (Fig. 1D). The TEM result also showed many hollow pores on FC NPs, which provided fixed space for the loading of ATX. As determined by dynamic light scattering (DLS) (Fig. 1E) and ultraviolet absorption (Figs. S1 and S2 in Supporting information), the FC-ATX NPs (FUC:COS:ATX = 1:1:0.1) had the smallest average particle size (size = 168.80 ± 5.15 nm), uniform size distribution (polydispersity index (PDI) = 0.13 ± 0.01), negative surface charge (zeta = −13.95 ± 1.05 mV), high ATX encapsulation efficiency (EE = 86.20% ± 2.10%) and loading efficiency (LE = 5.97% ± 0.71%). Therefore, FC-ATX NPs with a FUC:COS:ATX ratio of 1:1:0.1 was selected for subsequent experiments. The morphology of FC-ATX NPs was observed through TEM and illustrated the nanoparticles exhibiting the Tyndall effect when laser passed through them (Fig. 1F). Additionally, the morphology of FC-ATX NPs was characterized by field emission-scanning electron microscopy (FE-SEM) (Fig. S3 in Supporting information), showing clear morphology and size. Interestingly, both TEM and FE-SEM images revealed an elliptical shell surrounding the nanoparticles, making them resemble a pea pod. This unique morphology could be attributed to the strong negative charge of FC-ATX NPs, with positively charged COS aggregating around the nanoparticles due to electrostatic adsorption, similar to the reported dragon eye-like structure [44].

The binding of FUC and COS was further confirmed through Fourier-transform infrared spectroscopy (FT-IR) (Fig. S4 in Supporting information). The FT-IR spectrum of FUC displayed characteristic peaks at 848 and 1268 cm^{-1} corresponding to the stretching vibrations of C-O-S and S=O in FUC [36], while peaks at 1070, 1517, and 1625 cm^{-1} reached to the stretching vibrations of C–N and C=O in COS [39]. ATX encapsulation was confirmed by more substantial peaks at 968 and 1656 cm^{-1} in FC-ATX NPs spectra. In the differential scanning calorimetry (DSC), thermograms of ATX, FC NPs, and FC-ATX NPs (Fig. S5 in Supporting information) revealed a sharp endothermic peak at approximately 225 °C for pure ATX, indicating the melting of crystalline carotenoids. In contrast, a small endothermic peak at around 220 °C was observed for FC-ATX NPs [38]. ATX may be embedded in the micro-pores of the nanocarriers based on TEM images. Thus, some surface-embedded ATX would cause a slight endothermic peak. X-ray diffraction (XRD) measurements of FC-ATX NPs showed no pronounced crystalline peaks (Fig. S6 in Supporting information), indicating that ATX was encapsulated in FC-ATX NPs [45]. These results suggested that ATX successfully interacted with FUC and COS to form nanometer par-

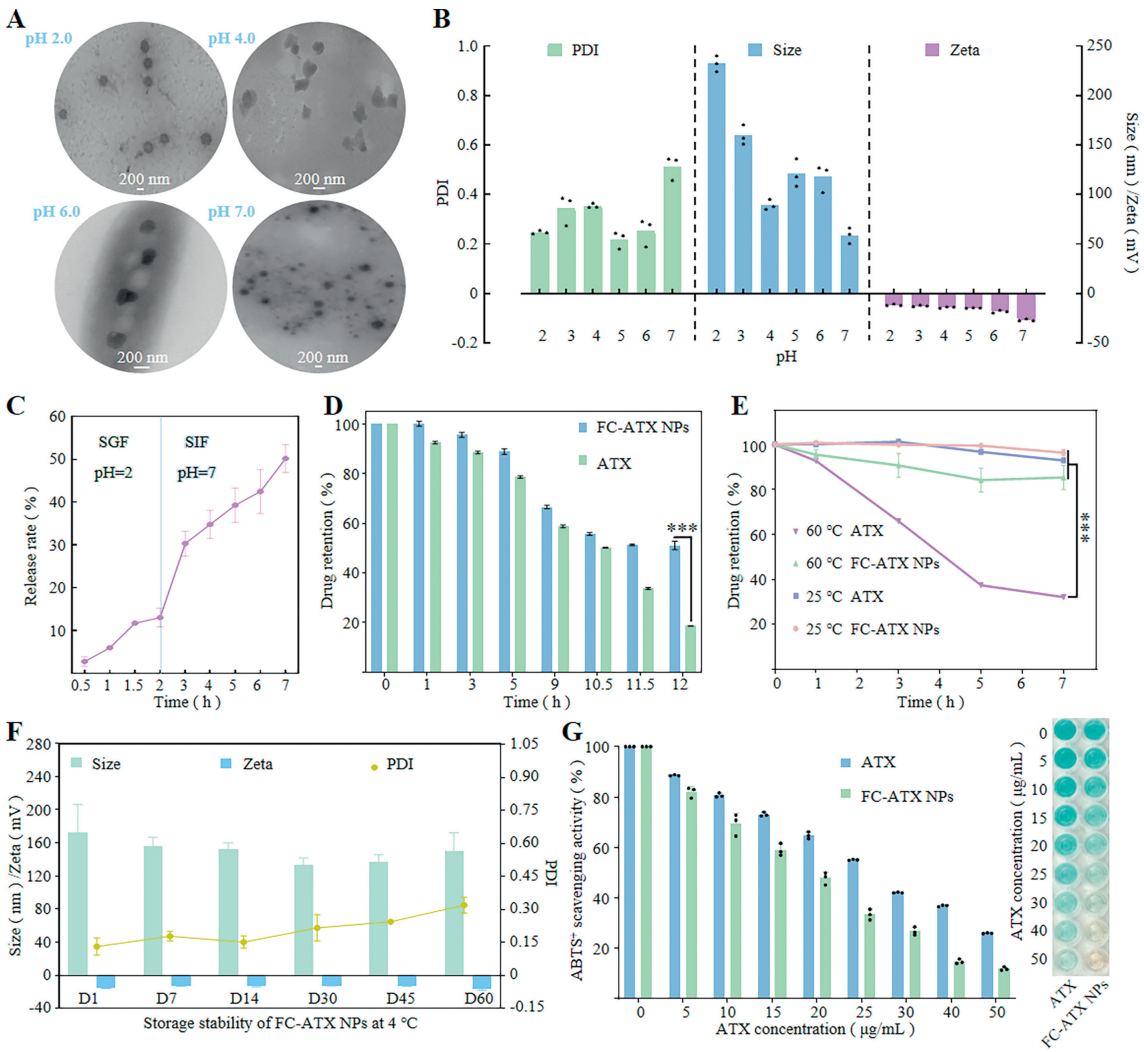

Fig. 2. Material stability. (A) The TEM images of FC-ATX NPs under different pH conditions. (B) DLS of FC-ATX NPs under different pH conditions. (C) Simulation of the gastrointestinal release of FC-ATX NPs. (D) The UV stability of FC-ATX NPs. (E) Thermal stability of FC-ATX NPs. (F) Storage stability of FC-ATX NPs at 4 °C. (G) $ABTS^{+}$ activity of FC-ATX NPs. $^{***}P < 0.001$. All data are presented by mean ± SD ($n = 3$).

ticles, and the prepared FC-ATX NPs did not change the structure of ATX.

The size, zeta potential, PDI, and TEM morphology of FC-ATX NPs were measured under different pH conditions (Figs. 2A and B). It could be observed that the particle size and PDI of FC-ATX NPs significantly increased at pH 2.0 but still maintained a relatively intact particle shape (size = 232.00 ± 8.00 nm, PDI = 0.25 ± 0.01). This might be due to the p*Ka* value of sulfate groups on FUC, which is approximately 1.0–2.5. These groups weaken the electrostatic interaction between FUC and COS in a pH 2.0 environment, resulting in nanoparticle expansion and the disappearance of the pod-like structure on the particle surface [46]. When the pH was 7.0, the electrostatic interaction between FUC and COS was nearly eliminated, and the nanoscale system was virtually destroyed (size = 58.19 ± 7.88 nm, PDI = 0.50 ± 0.04). TEM and DLS data at different pH values verified the pH-responsive release performance of the nanoparticles. Furthermore, the *in vitro* simulated digestion of FC-ATX NPs was studied using simulated gastric fluid (SGF, pH 2.0) and intestinal fluid (SIF, pH 7.0) [47]. NPs released 11.72% of ATX from SGF after 2 h, and the release rate significantly increased in SIF containing pancreatin, with 52.08% of ATX released after 5 h (Fig. 2C). The slow release of FC-ATX NPs in simulated gastric fluid demonstrates their suitability for intestinal targeting and controlled release, rendering them well-suited for oral administration.

The UV stability of ATX and FC-ATX NPs was determined with an enzyme-labeling instrument (Fig. 2D). The retention rate of free ATX decreased to 18.57% ± 0.12% after 12 h, while the retention rate of ATX in FC-ATX NPs remained at 50.87% ± 1.65%. The thermal stability curves of ATX and FC-ATX NPs at 25 and 60 °C were constructed based on absorbance measurement (Fig. 2E). FC-ATX NPs exhibited good thermal stability at both temperatures. Free ATX retained only 32.14% ± 0.18% of its content after 7 h at 60 °C. These results indicated that FC-ATX NPs could significantly improve the UV stability and thermal stability of ATX, providing a new strategy for delivering and applying poorly stable natural bioactive compounds. Long-term stability is crucial for the use of nanoparticles in the body. The particle size stability of FC-ATX NPs stored under light-shielding conditions at 4 °C (Fig. 2F) and 25 °C (Fig. S7 in Supporting information) for 60 and 30 days

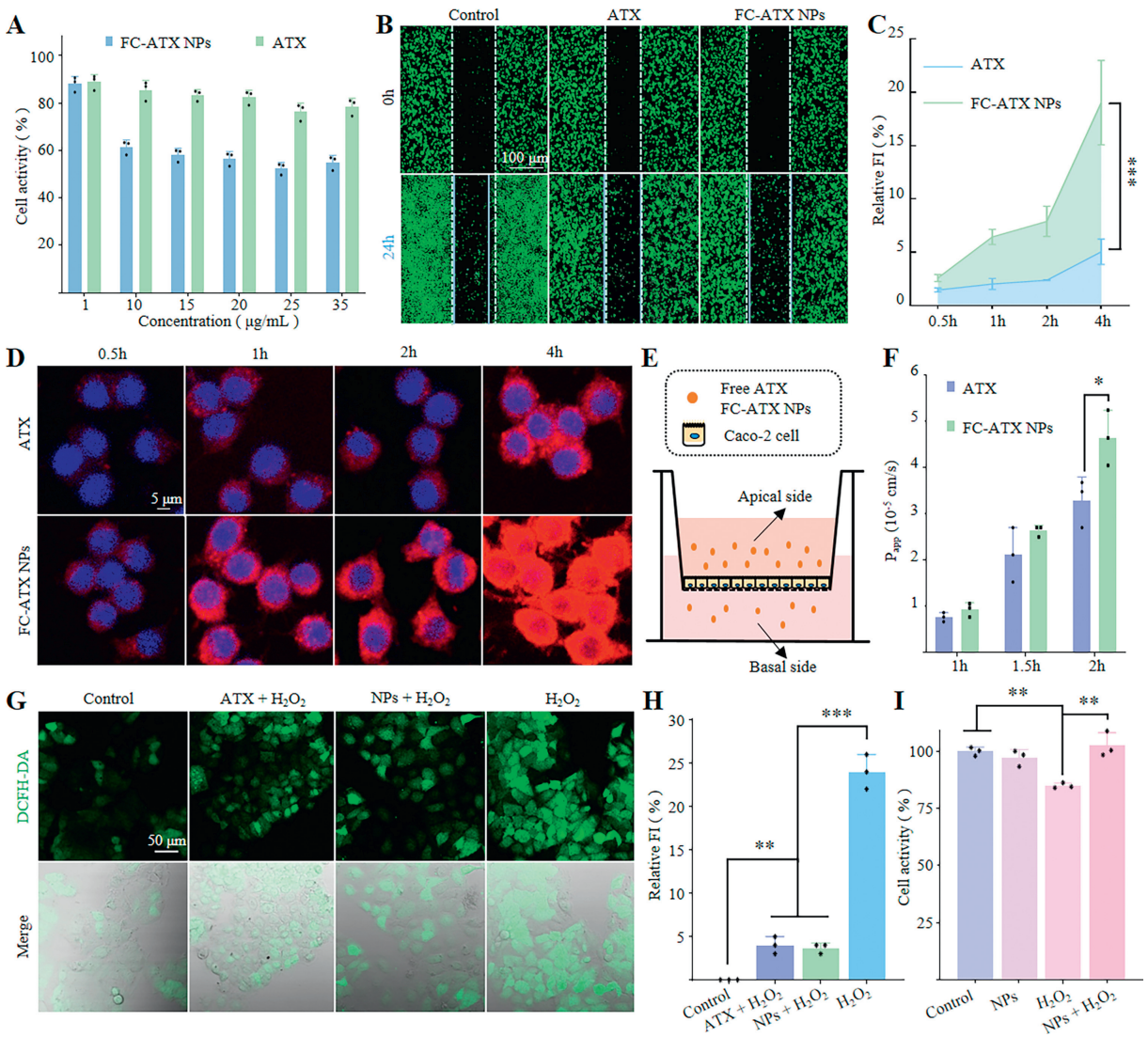

Fig. 3. Cell assays. (A) The toxicity of FC-ATX NPs in RAW 264.7 cells. (B) Images of RAW 264.7 cells wound healing assays at 0 and 24 h. (C) Relative fluorescence intensity analysis of cellular uptake. (D) Cellular uptake of FC-ATX NPs in RAW 264.7 cells. (E) Caco-2 monolayer transport of FC-ATX NPs. (F) Quantitative analysis of FC-ATX NPs monolayer transport. (G) Fluorescence images of intracellular ROS. (H) Relative fluorescence intensity of intracellular ROS. (I) Relative cell viability of Caco-2 cells under H_2O_2 with/without FC-ATX NPs. $^{*}P < 0.05$, $^{**}P < 0.01$, $^{***}P < 0.001$. All data are presented by mean ± SD ($n = 3$).

demonstrated good strength. FC NPs stored under light-shielding conditions at 25 °C (Fig. S8 in Supporting information) and 4 °C (Fig. S9 in Supporting information) also exhibited good storage stability within 30 days, providing options for delivering other drugs. Natural astaxanthin possesses a strong antioxidant capacity and can effectively reduce the production of ROS [48]. The free radical scavenging ability of the corresponding materials was detected through the 2,2′-azino-bis(3-ethylbenzothiazoline-6-sulfonate) radical cation ($ABTS^+$) clearance assay. The $ABTS^+$ extreme scavenging ability of ATX and FC-ATX NPs increased with increasing concentrations of ATX (Fig. 2G). It was evident that FC-ATX NPs exhibited higher clearance ability than free ATX (retention rate of 26.03% ± 0.18% when the ATX concentration was 50 μg/mL). This might be due to the antioxidant activity of FUC and COS present in FC-ATX NPs and the enhanced water solubility of ATX, resulting in improved antioxidant activity of the material [23,49].

Cell viability was measured using the MTT assay on Caco-2 cells (Fig. S10 in Supporting information) and RAW 264.7 cells (Fig. 3A), revealing that the cell toxicity of the FC-ATX NPs group was significantly higher than that of the free ATX group with the increase of ATX. The scratch test on RAW 264.7 cells also confirmed the excellent cytotoxicity of FC-ATX NPs (Fig. 3B). Dir was used instead of astaxanthin in uptake experiments to explore cellular uptake. Confocal images and fluorescence quantification of Dir and FC-Dir NPs demonstrated a more vital uptake capacity of FC-Dir NPs in RAW 264.7 cells (Figs. 3C and D). A Caco-2 monolayer transport model was used to investigate the *in vitro* permeation and transfer of ATX and FC-ATX NPs (Figs. 3E and F). After incubating Caco-2 cells with a monolayer model for 21 days [50], equal concentrations of ATX or FC-ATX NPs were added to the lower chamber of the culture media. The change in astaxanthin content in the lower chamber regular culture medium indicated its corresponding transport capacity. It can be seen that both ATX and FC-ATX NPs could transport through the Caco-2 cell monolayer to the lower chamber with time. Still, FC-ATX NPs exhibited higher apparent permeability coefficient (P_{app}) values than the ATX group, indicating enhanced membrane transportability of ATX in the Caco-2 monolayer.

ROS scavenging ability was performed by stimulating Caco-2 cells with H_2O_2 [51], which generates a large amount of ROS within cells (Figs. 3G and H). The fluorescence intensity of DCFH-

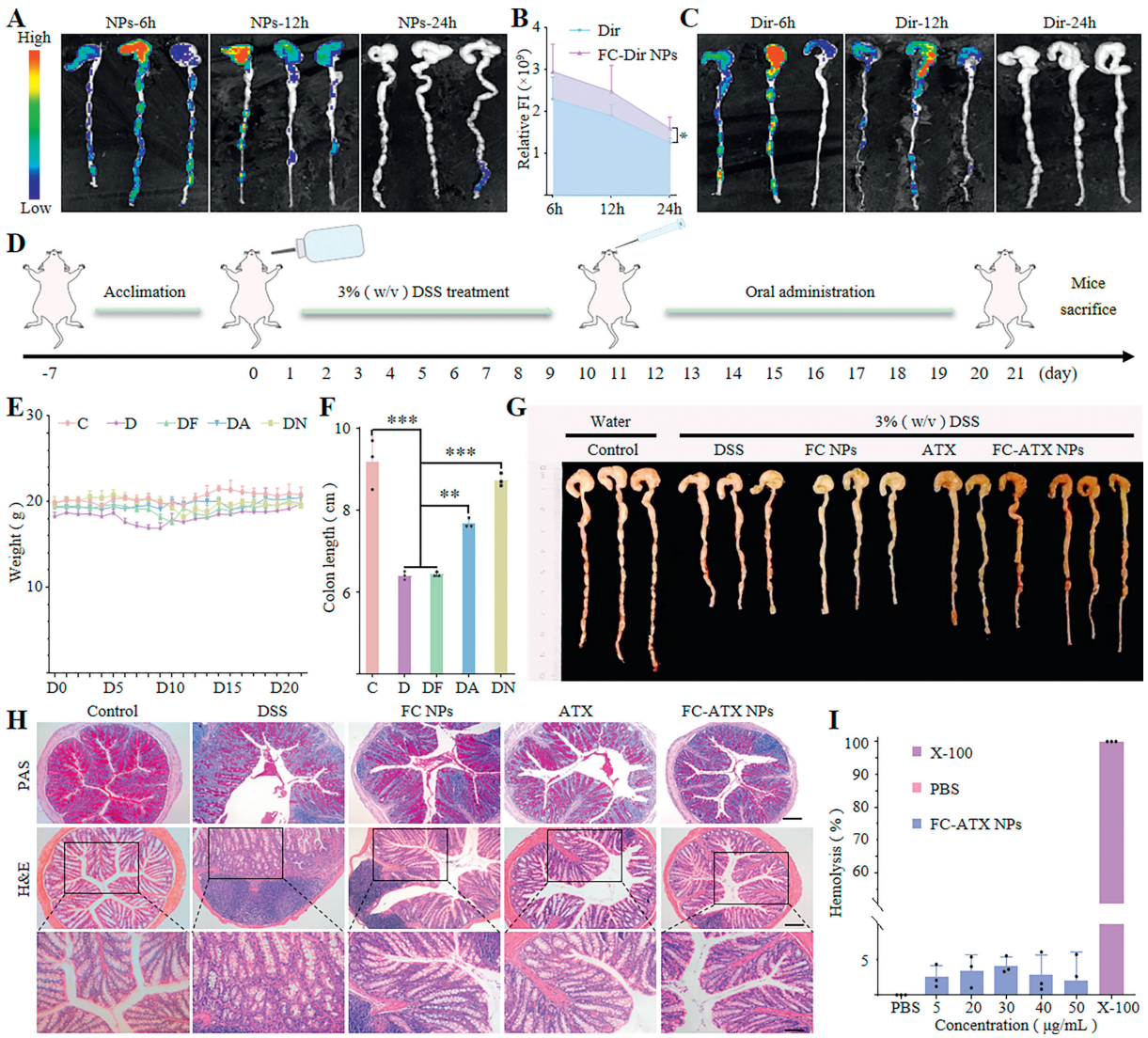

Fig. 4. *In vivo* therapy of colitis mice with FC-ATX NPs. (A–C) *Ex vivo* images of the colon in mice after orally administrated FC-Dir NPs and Dir. (D) The therapeutic course of colitis mice. (E) Body weight of mice during the therapy (C: control, D: DSS, DF: FC NPs, DA: ATX, DN: FC-ATX NPs). (F) Length of the colon after therapy. (G) Photo of the colon after therapy. (H) PAS and H&E staining sections of different therapy groups. Scale bars = 100 μm; Zoom area = 50 μm. (I) Different proportions of hemolysis rate of FC-ATX NPs. $^{**}P < 0.01$, $^{***}P < 0.001$. All data are presented by mean ± SD ($n = 3$).

DA was significantly lower in Caco-2 cells pre-incubated with ATX and FC-ATX NPs than those directly incubated with H_2O_2, indicating that astaxanthin can effectively eliminate the majority of ROS induced by H_2O_2. Furthermore, RAW 264.7 cells were used to demonstrate the reduction of oxidative damage caused by LPS by FC-ATX NPs (Fig. S11 in Supporting information). Additionally, the impact of H_2O_2 on relative cell activity in Caco-2 cells was evaluated using the MTT assay (Fig. 3I). The relative movement of Caco-2 cells incubated with H_2O_2 was lower than normal cells. In contrast, cells incubated with FC-ATX NPs exhibited good cell viability even when co-cultured with H_2O_2, showing significantly higher relative activity than cells cultured with H_2O_2 alone. These results indicate that ATX and FC-ATX NPs can effectively clear ROS, and FC-ATX NPs provide protection against cell death induced by oxidative stress.

Significant constraints for oral formulations include biodistribution and transit time in the gastrointestinal tract [52]. Hence, prolonging drug retention and transit time will improve mucosal contact and absorption. DSS-induced mice were orally administered with FC-Dir NPs, and free Dir was used as the control group. Imaging and quantitative results showed that oral administration of FC-Dir NPs exhibited stronger fluorescent signals in the colon region at 6–24 h (Figs. 4A–C). And the 12 h gastrointestinal fluorescence analysis results of FC-Dir NPs were also stronger than those of the Dir group (Figs. S12 and S13 in Supporting information), the above results indicated an excellent colon-targeting ability of FC-Dir NPs.

To evaluate the therapeutic effect of oral administration of FC-ATX NPs on mice with colitis induced by DSS, a mouse colitis model was employed (Fig. 4D). After 10 days of 3% DSS induction, all groups of mice, except the regular control group, experienced varying degrees of weight loss. Subsequently, following oral therapy with FC NPs, ATX, and FC-ATX NPs for 10 days, the body weight of mice in all groups returned to normal levels (Fig. 4E). The colon length (Fig. 4F) and images (Fig. 4G) after therapy indicated that both free ATX and FC-ATX NPs alleviated the issue of colonic shortening caused by colitis, with better therapeutic efficacy observed in the FC-ATX NPs group. Photos of isolated organs proved that the material has no obvious toxic side effects (Fig. S14 in Supporting information). Furthermore, observation of periodic acid schiff (PAS) and hematoxylin and eosin (H&E) stained colon tissue sections from different therapy groups (Fig. 4H) revealed that the DSS-treated group exhibited altered crypt structure, reduced goblet cells, and significant macrophage infiltration compared to the control group. However, both the free ATX group and FC-ATX NPs group mitigated the severity of inflammation compared to the DSS group, with the FC-ATX NPs group showing nearly typical tissue structure and a significant reduction in macrophage infiltration. Hemolysis experiments with different concentrations of FC-ATX NPs (Fig. 4I) demonstrated that the hemolysis rate did not exceed 5% with increasing FC-ATX NPs concentration, indicating good biocompatibility. These results show that FC-ATX NPs can accurately deliver ATX to the colon in mice. All animal experiments were conducted in strict compliance with the laws and institutional guidelines of Southwest University and approved by the Ethics Committee at Southwest University, Chongqing, China (No. LAC2023–1-0230).

This study established the pH-triggered release nano delivery system to encapsulate ATX through the ultrasound-assisted self-assembly of FUC and COS. The obtained FC-ATX NPs exhibited a distinctive “pod” structure, uniform size, high encapsulation efficiency, excellent physicochemical stability, pH-triggered colon-targeted sustained release properties, and potent antioxidant capacity. They effectively alleviated DSS-induced colitis symptoms and demonstrated good biocompatibility. Overall, pH-responsive FC-ATX NPs provide a practical approach to enhance the bioavailability of ATX and have great potential as an oral nutritional delivery system for colitis therapy.

Declaration of competing interest

The authors declare that they have no known competing financial interests or personal relationships that could have appeared to influence the work reported in this paper.

Acknowledgments

This work was financially supported by the Chongqing Graduate Program of Research and Innovation (No. CYS22207), the National Natural Science Foundation of China (No. 51703187), and Chongqing Talents of Exceptional Young Talents Project, China (Nos. CQYC202005029 and cstc2021ycjh-bgzxm0061).

Supplementary materials

Supplementary material associated with this article can be found, in the online version, at doi:10.1016/j.cclet.2023.109029.

References

[1] X. Zhang, X. Zhao, Z. Hua, et al., Biomaterials 292 (2022) 121937.
[2] Y. Chen, W. Su, S. Tie, et al., Biomaterials 293 (2023) 121976.
[3] L.C. Yu, J. Biomed. Sci. 25 (2018) 79.
[4] B. Yang, Y. Chen, J. Shi, Chem. Rev. 119 (2019) 4881–4985.
[5] R. Mittler, Trends Plant Sci. 22 (2017) 11–19.
[6] C. Zhang, J. Li, M. Xiao, et al., Chin. Chem. Lett. 33 (2022) 4924–4929.
[7] H. Wang, X. Zhang, W. Zhu, Y. Jiang, Z. Zhang, Ind. Eng. Chem. Res. 57 (2018) 12689–12699.
[8] T. Nie, Z. He, J. Zhu, L. Liu, Y. Chen, Adv. Therapeutics 3 (2020) 2000016.
[9] Y. Qin, R. Zhao, H. Qin, et al., Nano Today 39 (2021) 101234.
[10] Y. Cui, T. Zhu, X. Zhang, et al., Chin. Chem. Lett. 33 (2022) 4617–4622.
[11] X. Wang, C. Ding, Z. Zhang, et al., Chin. Chem. Lett. 34 (2023) 107951.
[12] X. Li, M. Ye, Y.E. Gao, et al., Adv. Fiber Mater. 4 (2022) 1141–1152.
[13] M.Y. Liang, M.J. Zhang, W. Qiu, et al., Adv. Sci. 9 (2022) 2203353.
[14] T. Nie, Z. He, Y. Zhou, et al., ACS Appl. Mater. Inter. 11 (2019) 29593–29603.
[15] R.R. Ambati, S.M. Phang, S. Ravi, R.G. Aswathanarayana, Mar. Drugs 12 (2014) 128–152.
[16] R. Edelman, S. Engelberg, L. Fahoum, E.G. Meyron-Holtz, Y.D. Livney, Food Hydrocoll. 96 (2019) 72–80.
[17] S. Fakhri, F. Abbaszadeh, L. Dargahi, M. Jorjani, Pharmacol. Res. 136 (2018) 1–20.
[18] I. Higuera-Ciapara, L. Felix-Valenzuela, F.M. Goycoolea, Crit. Rev. Food Sci. Nutr. 46 (2006) 185–196.
[19] D. Zhang, J. He, J. Cui, et al., ACS Nano 17 (2023) 10560–10576.
[20] C. Yang, Y.I. Hassan, R. Liu, et al., J. Agric. Food Chem. 67 (2019) 6222–6231.
[21] X. Zhang, X. Zhao, S. Tie, H. Wang, M. Tan, J. Agric. Food Chem. 69 (2021) 2719–2728.
[22] X. Liu, D.J. McClements, Y. Cao, H. Xiao, Food Biophys. 11 (2016) 302–310.
[23] H.D. Choi, H.E. Kang, S.H. Yang, M.G. Lee, W.G. Shin, Br. J. Nutr. 105 (2011) 220–227.
[24] L. Huang, D. Li, Y. Ma, et al., Food Hydrocoll. 123 (2022) 107152.
[25] V. Rodriguez-Ruiz, J.A. Salatti-Dorado, A. Barzegari, et al., Molecules 23 (2018) 2601.
[26] H. Yu, H. Wang, W. Su, et al., Food Hydrocoll. 131 (2022) 107810.
[27] X. Zhang, X. Zhao, S. Tie, et al., J. Control. Release 342 (2022) 372–387.
[28] T. Nie, Z. Fang, H. Liu, et al., Chem. Eng. J. 446 (2022) 137353.
[29] J. Zhao, W. Gao, X. Cai, et al., Theranostics 9 (2019) 2843–2855.
[30] I.P.S. Fernando, D. Kim, J.W. Nah, Y.J. Jeon, Chem. Eng. J. 355 (2019) 33–48.
[31] X. Yu, C. Wang, Y. Wang, et al., Front. Chem. 10 (2022) 838920.
[32] C.H. Chung, K.Y. Lu, W.C. Lee, et al., Biomaterials 257 (2020) 120227.
[33] X. Zhang, Z. Wei, C. Xue, Crit. Rev. Food Sci. Nutr. 62 (2021) 8935–8953.
[34] G. Despras, A. Alix, D. Urban, B. Vauzeilles, J.M. Beau, Ange. Chem. Int. Ed. 53 (2014) 11912–11916.
[35] X. Li, C. Yin, B. Liu, et al., Food Hydrocoll. 134 (2023) 107996.
[36] Y.C. Huang, T.H. Kuo, Food Hydrocoll. 53 (2016) 261–269.
[37] C. Wu, J. Sun, H. Jiang, Y. Li, J. Pang, Food Chem. 362 (2021) 130242.
[38] C. Liu, S. Zhang, D.J. McClements, D. Wang, Y. Xu, J. Agric. Food Chem. 67 (2019) 5113–5121.
[39] H. Wang, L. Hu, J. Du, et al., Food Hydrocoll. 121 (2021) 107050.
[40] C. Liu, Z. Liu, X. Sun, et al., J. Agric. Food Chem. 66 (2018) 6717–6726.
[41] F.N. Sorasitthiyanukarn, C. Muangnoi, P. Rojsitthisak, P. Rojsitthisak, Food Hydrocoll. 124 (2022) 107246.
[42] M.W. TM, W.M. Lau, V.V. Khutoryanskiy, Polymers (10) (2018) 267.
[43] S.W. Zhu, M. Ye, X. Ma, et al., Acta Biomater. 154 (2022) 497–509.
[44] W. Bao, X. Liu, Y. Lv, et al., ACS Nano 13 (2019) 260–273.

[45] F. Yu, J. Chen, Z. Wei, et al., Front. Nutr. 9 (2022) 1022323.
[46] Y.C. Huang, R.Y. Li, Mar. Drugs 12 (2014) 4379–4398.
[47] M. Sabaghi, S. Tavasoli, S.Z. Hoseyni, et al., Food Chem. 382 (2022) 132411.
[48] Y. Chen, W. Su, S. Tie, L. Zhang, M. Tan, Trends Food Sci. Tech. 127 (2022) 63–73.
[49] A.F. Hifney, M.A. Fawzy, K.M. Abdel-Gawad, M. Gomaa, Food Hydrocoll. 54 (2016) 77–88.
[50] X. Shen, C. Zhao, J. Lu, M. Guo, J. Agric. Food Chem. 66 (2018) 1472–1478.
[51] R. Zhang, L. Cheng, Z. Dong, et al., Mater. Horiz. 8 (2021) 1314–1322.
[52] Z. Le, Z. He, H. Liu, et al., Biomater. Sci. 10 (2022) 4156–4169.